Computational Investigation of Glycosylase and β-Lyase Activity Facilitated by Proline: Applications to FPG and Comparisons to hOgg1

ARTICLE *in* THE JOURNAL OF PHYSICAL CHEMISTRY B · NOVEMBER 2014

Impact Factor: 3.3 · DOI: 10.1021/jp507783d · Source: PubMed

2 AUTHORS, INCLUDING:

Shahin Sowlati Hashjin
University of Lethbridge
10 PUBLICATIONS **19** CITATIONS

THE JOURNAL OF PHYSICAL CHEMISTRY B

Article

pubs.acs.org/JPCB

Computational Investigation of Glycosylase and β-Lyase Activity Facilitated by Proline: Applications to FPG and Comparisons to hOgg1

Shahin Sowlati-Hashjin and Stacey D. Wetmore*

Department of Chemistry and Biochemistry, University of Lethbridge, 4401 University Drive West, Lethbridge, Alberta T1K 3M4, Canada

Supporting Information

ABSTRACT: Quantum mechanical methods are used to investigate the chemical steps during the bifunctional (glycosylase and β-lyase) activity of bacterial FPG DNA glycosylase, which removes the major oxidation product (8-oxoguanine) from DNA as part of the base excision repair process. To facilitate investigation of all potential pathways, the smallest chemically relevant model is implemented, namely a modified OG nucleoside-3′-monophosphate and a truncated proline nucleophile. Potential energy surfaces are characterized with SMD-M06-2X/6-311+G(2df,2p)//PCM-B3LYP/6-31G(d) and compared to a previous study on the analogues human enzyme (hOgg1), which uses a lysine nucleophile (Kellie, J. L.; Wetmore, S. D. *J. Phys. Chem. B* **2012**, *116*, 10786−10797). Our large calculated barriers indicate that FPG must actively catalyze the three main phases of the overall reaction, namely, deglycosylation, (deoxyribose) ring-opening, and β-elimination, and provide clues about how this is achieved through comparison to accurate crystal structures. The main conclusions about key mechanistic steps hold true regardless of the nucleophile, suggesting that most major differences in the relative activity of FPG and hOgg1 are primarily due to other active site residues. Nevertheless, support for possible monofunctional (deglycosylation only) activity is only evident when lysine is the nucleophile. This finding agrees with experimental observations of monofunctional activity of hOgg1 and further supports the broadly accepted bifunctional activity of FPG.

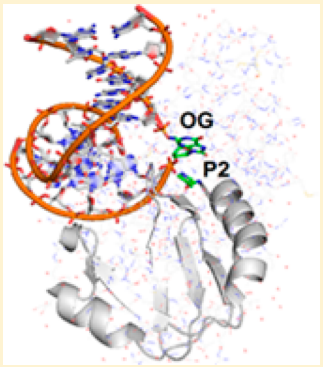

INTRODUCTION

DNA undergoes many different types of damage due to exposure to carcinogenic substances, reactive oxygen species (ROS) and high-energy radiation.[1] Although alterations can occur to the sugar−phosphate backbone, damage to one of the four native nucleobases is more frequent. DNA nucleobase lesions can generally be divided into two broad categories, known as bulky and nonbulky damage. Nonbulky damage changes few atoms in a canonical nucleobase and includes examples such as deamination of cytosine (C) to uracil (U) and oxidation of guanine (G) to 8-oxoguanine (OG). The formation of OG is the overall most common DNA damaging event,[2] occurring approximately 10^3 times per day per cell.[3−5] Although OG retains Watson−Crick (WC) interactions with C in a DNA helix when in the *anti* conformation (χ, which is defined as ∠(O4′−C1′−N9−C4) for the purines, equals 180 ± 90°), OG can also rotate about the glycosidic bond to adopt the *syn* conformation (χ = 0 ± 90°), which can form a stable Hoogsteen base pair with adenine (A). In fact, OG shows a preference for the OG:A pairing pattern,[6−8] which in turn leads to a G:C → T:A transversion mutation after two rounds of replication. This transversion mutation is among the most common mutations in cells associated with lung, breast, ovarian, colorectal, and renal cancers.[9]

Nonbulky damage is generally repaired through the base excision repair (BER) pathway. BER is initiated when a glycosylase scans the DNA backbone and identifies a damaged nucleobase. The lesion is flipped out of the helix and into the active site of the glycosylase. Next, nucleotide deglycosylation occurs, which breaks the glycosidic bond between the damaged nucleobase and the deoxyribose moiety to produce an abasic site (also known as an apyrimidinic/apurinic (AP) site). Based on the activity mode, DNA glycosylases can be divided into two broad classes, namely, monofunctional and bifunctional enzymes. While monofunctional glycosylases only catalyze deglycosylation, bifunctional glycosylases are also capable of nicking the 3′-side of the DNA backbone (β-lyase activity), a role played by an AP-endonuclease when a monofunctional glycosylase facilitates the first repair step. Another important difference between the two classes of glycosylases is the nucleophile used to break the glycosidic bond, which is generally a water molecule for the monofunctional enzymes and an active site amine for the bifunctional enzymes. The repair process is completed when a DNA polymerase adds the native nucleotide and a DNA ligase seals the strand.

The bifunctional human 8-oxoguanine−DNA glycosylase (hOgg1) and its bacterial counterpart formamidopyrimidine-DNA glycosylase (FPG or MutM) are responsible for excising

Received: August 1, 2014
Revised: October 13, 2014
Published: November 21, 2014

dx.doi.org/10.1021/jp507783d | *J. Phys. Chem. B* 2014, 118, 14566−14577

OG. The generally accepted chemical steps utilized in the bifunctional activity of these enzymes are shown in Scheme 1.[10−12] The first step involves nucleophilic attack (by proline in FPG and lysine in hOgg1), which displaces OG. This is followed by the ring-opening step, which is initiated by (direct or general base-assisted) proton transfer from the amine nucleophile to O4′ in deoxyribose, leading to a Schiff base intermediate. Although one study suggests that ring-opening may occur prior to deglycosylation,[13] ring-opening occurs after deglycosylation in the most broadly accepted mechanism.[10−12] Next, β-lyase activity occurs through proton abstraction from C2′ by a general base, resulting in 3′-phosphate elimination. The final step recovers the enzyme through hydrolysis of the Schiff base and leaves the nicked DNA strand for further processing.

Scheme 1. General Steps during dOG Deglycosylation and β-Elimination Catalyzed by hOgg1 (Nuc−H = Lysine) and FPG (Nuc−H = Proline) Including (a) Base Displacement, (b) Ring-Opening via Proton Transfer from Nα to O4′ and Consequent Schiff Base Formation, (c) Proton Abstraction from C2′ Followed by 3′ Backbone Cleavage, and (d) Hydrolysis of the Crosslink to Generate the Nicked Product and the Enzyme

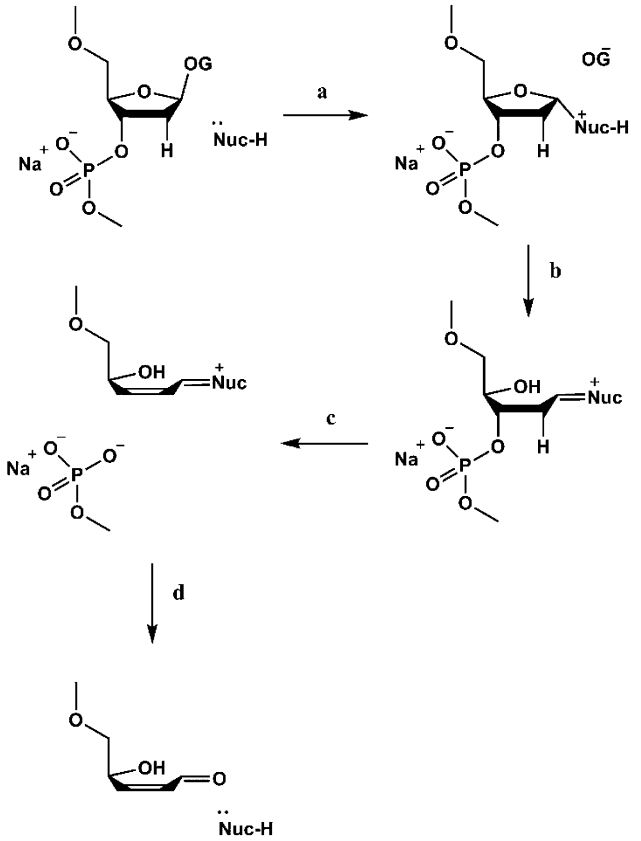

Experimental studies on hOgg1 have confirmed the key catalytic role of Lys249 as the nucleophile,[14−17] and have established that Asp268 is also catalytically essential, the main role being electrostatic stabilization of the Schiff base intermediate.[15,16] However, debate surrounding the activity mode of the enzyme exists in the literature, with several studies showing that hOgg1 can behave as a monofunctional enzyme in vivo.[18−23] Support for this proposal comes from Dalhus and co-workers who found that placing Lys249 far from C1′ does not inhibit glycosylase activity.[16] Previous computational studies of the chemical step catalyzed by hOgg1 have primarily focused on the deglycosylation phase,[24−28] with only select studies considering the ring-opening step.[24,26] Most recently, Kellie and Wetmore have mapped several possible pathways for the hOgg1 bifunctional mode using the smallest chemically relevant model (a modified (*anti*) nucleoside-3′-monophosphate and a truncated lysine nucleophile).[29] In fact, this was the first computational study to consider the lyase reaction facilitated by a bifunctional glycosylase. Interestingly, this work also supports the proposed monofunctional activity of hOgg1 by identifying the low energy intermediate as the DNA−protein cross-link that occurs before ring-opening, but after proton transfer from the amine, which would lead to monofunctional activity if hydrolyzed.

Despite sharing the main phases of the BER process (Scheme 1), hOgg1 and FPG are different in several respects. First, although hOgg1 and FPG employ a similar "direct readout" mechanism[30] to identify damaged lesions through hydrogen-bonding or electrostatic interactions, each enzyme employs different active site residues.[11,31] As a result, although hOgg1 primarily excises OG, FPG displaces several other types of damaged nucleobases, including 2,6-diamino-4-hydroxy-5-formamidopyrimidine (FapyG), thymine glycol (Tg), dihydrouracil (DHU), and 5-hydroxyuracil (5-OHU), as well as hydantoins.[32−36] Second, despite both enzymes utilizing a terminal amine to displace OG, the difference in the identity of the nucleophile affects reactivity. Specifically, the catalytic proline used by FPG leads to only one proton abstraction (Nα) possibility from the nucleophile following deglycosylation compared with two possibilities afforded by lysine (Nε) in hOgg1. Third, although the free OG generated upon deglycosylation may act as a cofactor for O3′-elimination in the active site of hOgg1,[12] there is evidence that the excised OG is not tightly bound to FPG,[10] which may change the mechanism of subsequent chemical steps. Finally, in addition to β-lyase activity, FPG uniquely possesses δ-lyase activity or, in other words, is also capable of nicking the 5′-side of the DNA backbone.[37] Collectively, these differences lead to an 80-fold greater efficiency of FPG over hOgg1.[10,38]

Unfortunately, much less is known about the chemical steps employed in the mechanism of action of FPG compared to hOgg1. To date, most experimental studies on FPG have focused on the structure of the DNA−enzyme cross-link and the lesion recognition step,[11,39−41] with only a few investigations proposing mechanisms for the β-lyase[10,32,39] and δ-lyase steps.[32] Similarly, computational investigations of FPG are limited. Molecular dynamics (MD) studies on different conformations of the substrate, as well as a selection of other lesions,[42−45] in the recognition pocket have paralleled experimental work. Only one quantum mechanical study has used a truncated-enzymatic model to consider the catalytic mechanism, but only examined the deglycosylation step.[46]

To expand our knowledge of the mechanism employed by bifunctional glycosylases, and FPG in particular, the present study investigates potential deglycosylation to β-elimination mechanisms employed by FPG (Scheme 1). To allow the greatest number of pathways to be considered, the smallest chemically relevant model is employed, which includes a modified nucleoside-3′-monophosphate and truncated proline nucleophile. Although this model will not fully recover all details of the chemical reactions occurring in the FPG active site, this approach will reveal the intrinsically preferred

dx.doi.org/10.1021/jp507783d | J. Phys. Chem. B 2014, 118, 14566−14577

mechanisms of the main phases in the overall process. This will identify pathways that must be considered in future large-scale modeling of the enzymatic reaction, where investigating all mechanistic options is computationally prohibited. Furthermore, our model is equivalent to the model employed to investigate the bifunctional activity of hOgg1[29] (lysine as the nucleophile). Therefore, this will permit accurate comparison between the two enzymes in order to identify any differences in the inherent chemistry originating due to the nucleophile. Although comparing the efficiency of the human and bacterial enzymes is interesting from an evolutionary viewpoint, this comparison also has important applications in cancer treatments. For example, inhibitors for DNA repair enzymes have been shown to enhance the efficiency of cancer chemotherapeutic agents.[47−51] More specifically, bacterial FPG has been argued to be much more efficient than hOgg1 in protecting cultured human lung cells from oxidative damage.[47]

COMPUTATIONAL DETAILS

Model. Although many crystal structures are available for various FPG mutants and modified substrates (see, for example, refs 10, 11, 40, and 76), to the best of our knowledge, only one high-resolution structure is available with the enzyme bound to DNA containing an intact 8-oxoguanine nucleoside (PDB ID: 1R2Y).[11] Therefore, our starting models were based on this crystal structure. We note that, although the N-terminal formylmethionine is cleaved post-translationally in *Escherichia coli*,[52] the N-terminus is not cleaved in some mutant FPG enzymes,[53,54] which leads to the proline nucleophile being designated as residue 2. We adopt this convention in the present work to match the crystal structure numbering.

The initial geometry of *syn* dOG and the proline nucleophile (Pro2) was obtained from the crystal structure 1R2Y.[11] This choice for dOG ensures that structural changes to the DNA backbone inflicted when the glycosylase flips the base out of the DNA helix are taken into account. The *anti* conformer was generated by rotating dOG about the glycosidic bond and followed by a geometry optimization. In order to investigate the β-elimination step catalyzed by FPG, a modified nucleoside-3′-monophosphate is used (Figure 1) in which the 3′ and 5′-terminal oxygen atoms are capped by methyl (Me) groups rather than hydrogens to avoid artificial hydrogen bonds between a terminal hydrogen and the nucleobase, sugar or nucleophile that does not occur in DNA. Neglect of the C5′-phosphate is justified by a previous study showing that, although geometries may change slightly, the calculated energy barriers remain similar upon inclusion of this group.[55]

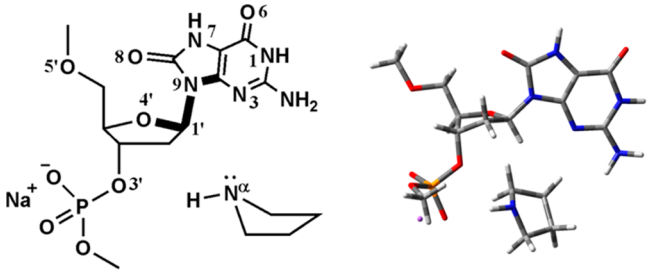

Figure 1. 2D (left) and 3D (right) representations of the computational model employed in the present study, which includes 3′-monophosphate dOG (capped with methyl groups at O5′ and the 3′ phosphate) and proline (modeled as pyrrolidine). A sodium counterion is included to charge neutralize the phosphate moiety. The χ dihedral angle ($\angle$(O4′−C1′−N9−C4)) is shown in bold.

To neutralize the model, a sodium ion was added equidistant to the oxygen atoms in the 3′-phosphate group, which has been shown to result in better geometries than protonated or anionic models.[56,57] We note that the effect of replacing the sodium ion with a potassium ion was considered for the elimination step since the metal ion likely plays the most important role in this step of the overall reaction. However, only slight changes to the calculated geometries were observed (<0.18 Å change in key bond lengths and ∼3.5° change in key angles; Figure S2, Supporting Information). As a result, the calculated energetics of this step were unaltered by changing the counterion, and a sodium ion was used to model the remaining reaction steps. The proline nucleophile is modeled as pyrrolidine (Figure 1). This model choice is consistent with the previous study that used a (truncated) lysine nucleophile.

Mechanisms. Although there is evidence that OG is not tightly bound in the FPG active site after excision,[10] OG has been proposed to be involved in subsequent (C2′−H abstraction) reaction steps.[12,58] Therefore, to bypass existing confusion in the literature regarding the identity of key catalytic residues, the excised OG plays the role of the general base and acid as required throughout the reaction pathway in the present work. Although other residues in the FPG active site likely fulfill these roles during the enzyme-catalyzed reaction, this choice allows us to maintain a small and consistent model throughout the reaction in order to consider all possible reaction pathways. Nevertheless, this function requires inevitable motion of OG at different mechanistic steps, which may deviate from accessible OG orientations in the FPG active site. Most importantly, the model implemented does not affect our main conclusions regarding the necessity of an active site base and acid to catalyze the various chemical steps. As a result, the small model provides important geometrical information that can be used in future large-scale modeling of the DNA−protein complex, which will accurately identify the roles of active site residues.

The pathways considered in the current study for the first three mechanistic steps in the bifunctional activity of FPG (Scheme 1) are schematically shown in Scheme 2. The first step (a) is dOG deglycosylation, producing a covalently bound DNA−protein cross-link and the OG anion. This step is considered for both the *syn* and *anti* conformations of dOG. In the second step (b), the abasic intermediate undergoes a Schiff base rearrangement through proton transfer from Nα of the original proline nucleophile to O4′ of deoxyribose, which leads to a ring-opened intermediate. This step can be accompanied by either direct proton transfer or proton transfer assisted by a general base and acid. In the direct pathway, the proton is directly transferred from Nα of proline to O4′ of the sugar, causing the ring to open. This pathway is considered for both the *anti* and *syn* conformations of dOG. In the assisted pathway, a base (OG in our model) first abstracts the proton from Nα, and subsequently delivers the proton to O4′. Proton abstraction is considered to be performed by O8 or N9 of OG in two separate pathways. The final step (c) is 3′-phosphate elimination through β-lyase activity. This phase begins with C2′−H abstraction, which is performed by O8 or N9 of OG, and requires translational motion of OG from the proximity of O4′ to C2′. This step is followed by the final 3′-phosphate elimination.

dx.doi.org/10.1021/jp507783d | J. Phys. Chem. B 2014, 118, 14566−14577

Scheme 2. Pathways Considered in the Present Study Including (a) Deglycosylation Initiated from Either the *anti* or *syn* Conformation of dOG, (b) Ring-Opening with Either Direct (from the *anti* or *syn* Conformer) or Base-Assisted Proton Transfer from Nα to O4′ (by N9 or O8 of the Excised OG), and (c) Elimination Coupled with Proton Abstraction by Either N9 or O8 of the Excised OG Followed by 3′-Phosphate Departure

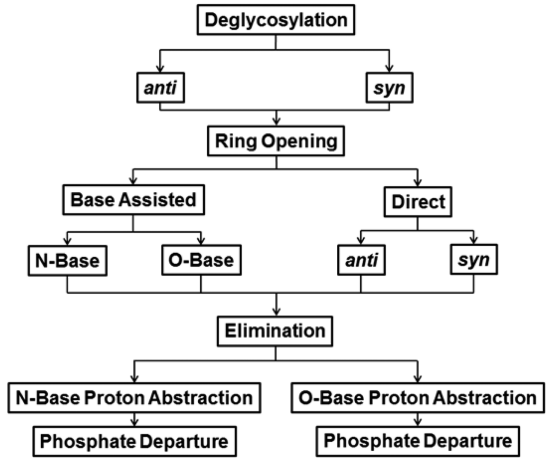

The nomenclature employed in a previous work on a lysine nucleophile (hOgg1)[29] is used in the present work to facilitate meaningful comparisons between the studies. Specifically, consistent with Scheme 1, the structures corresponding to the deglycosylation step end in (a), while stationary points referring to the ring-opening and elimination steps end in (b) and (c), respectively. For example, the transition state for the deglycosylation step is labeled TS(a), while the associated intermediate is denoted IC(a). When a mechanistic step involves more than one intermediate, a prime is used to distinguish between the structures. For example, the carbanion intermediate formed in the third reaction phase is denoted IC(c′).

Methodology. Reaction potential energy surfaces (PESs) were searched for each mechanistic pathway (Scheme 2) by optimizing the corresponding transition states (TS). Subsequently, the intrinsic reaction coordinate (IRC) was carefully followed as far as possible and the resulting structures were fully optimized to generate relaxed reactant, intermediate and product complexes. Within our model, the product of each chemical step may not exactly correspond to the reactant for the subsequent reaction. This is mainly because of inevitable translational motion of OG due to its multiple roles along the reaction pathway. Unfortunately, however, efforts to characterize transitions between the intermediates were not successful. Therefore, structures obtained from reverse IRCs were considered to be the intermediate that links the previous reaction step. Nevertheless, deviations in the structures primarily correspond to motion of the excised nucleobase, necessary for this residue to act as general base and acid, and therefore the major conclusions from our work will not be affected. Furthermore, the deglycosylation products are energetically and structurally the same as the reactants of the direct ring-opening reaction, with the energy difference falling within chemical accuracy (4 kJ/mol) for both the *anti* and *syn* dOG conformations.

All stationary points were fully optimized at the B3LYP/6-31G(d) level of theory in the presence of bulk solvent as described by the IEF-PCM method implemented in Gaussian 09.[59] Previous work shows that structural and energetic changes upon addition of diffuse functions are negligible for a similar reaction.[29] Frequency calculations were performed at the same level of theory to discern the nature of stationary points, and obtain zero-point vibrational and Gibbs free energy corrections. All single-point calculations were completed using SMD-M06-2*X*/6-311+G(2df,2p), which has been argued to perform well for S_N2 and elimination reactions.[60] To investigate the effects of basis set expansion on our calculated structures and energetics, we recalculated the lowest energy pathway with B3LYP/6-31G(d,p) (Table S1, Figure S1, and Cartesian coordinates S32−S39, Supporting Information). We find that basis set expansion generally leads to a relatively small change in the barriers height, with the largest effect occurring in the deglycosylation transition state (∼14 kJ/mol or less than 10%). Additionally, important geometrical features do not deviate significantly between the two basis sets, with the largest difference in bond length being 0.027 Å and the largest difference in bond or dihedral angle being 0.7°.

A wide range of dielectric responses have been predicted for different proteins by molecular simulation methods, which range from $\varepsilon \approx 3$ in the center of globular proteins to a gradual increase to 10 at protein boundaries.[61−66] Based on the shape of FPG and the location of the active site, the dielectric constant of diethyl ether (4.24) was to estimate the effects of the surrounding protein in all calculations. Although we acknowledge this estimation may not reflect the exact reaction environment, this approach is more accurate than gas-phase calculations. Unless otherwise mentioned, all reported energies correspond to (unscaled) Gibbs free energies obtained from the single-point calculations. All calculations were carried out using Gaussian 09 (revision C.01).[59]

RESULTS

The relative SMD-M06-2*X*/6-311+G(2df,2p) Gibbs free energies of the multiple pathways considered in the present study for the dOG glycosylase and β-lyase activity of FPG (Scheme 2) are provided in Table 1 and the corresponding Gibbs reaction surfaces are shown in Figure 2. Each step in the overall mechanism is separately considered directly below, while a comparison to hOgg1 and the biological implications will be addressed in the Discussion section. Due to the neglect of discrete active site residues in the computational model, the calculated energy barriers reported in the present study will vary from experimental barriers, with the magnitude of the effect potentially varying for each reaction step. Nevertheless, our model recovers several main geometrical features throughout the reaction as determined by comparison to experimental crystal structures. Therefore, the model implemented will fulfill our primary goal of obtaining information about the conformational flexibility of a large number of pathways, which can be used in future large-scale modeling of the entire DNA−protein complex.

Deglycosylation. Previous MD studies support both *anti* and *syn* conformations of dOG in DNA bound to FPG.[42,43] Although Amara et al. have shown that the *syn* conformation of dOG is favored in *Lactococcus lactis* models,[42] Simmerling et al. argue that this conformational preference arises from interactions with a nonconserved E77 residue.[43] Indeed, replacing E77 by serine, which occurs in *E. coli* and other

dx.doi.org/10.1021/jp507783d | J. Phys. Chem. B 2014, 118, 14566−14577

Table 1. Relative Gibbs Free Energies (kJ/mol) for Stationary Points Characterized along the Deglycosylation and β-Lyase Pathways Considered in the Present Work[a,b]

	Deglycosylation			
	anti		*syn*	
RC	0		4	
TS(a)	148.6		140.2	
	Ring-Opening			
	Direct		Assisted	
	Anti	*Syn*	O-base	N-base
IC(a)	36.9	25.4	−44.9	−11.5
TS(b)	180.8	178.7	−55.2	−13.7
IC(b′)	–		11.7	−58.9
TS(b′)	–		35.6	39.9
	Elimination			
	O-base proton abstraction		N-base proton abstraction	
IC(b)	51.4		38.6	
TS(c)	72.9		74.1	
	3′-PO_4 departure		3′-PO_4 departure	
IC(c′)	47.6		5.1	
TS(c′)	128.3		100.5	
IC(c)	94.7		65.4	

[a]Energies reported relative to a common (*anti*) reactant complex (Figure 1). [b]M06-2X/6-311+G(2df,2p)//PCM-B3LYP/6-31G(d) values including unscaled correction to Gibbs energy.

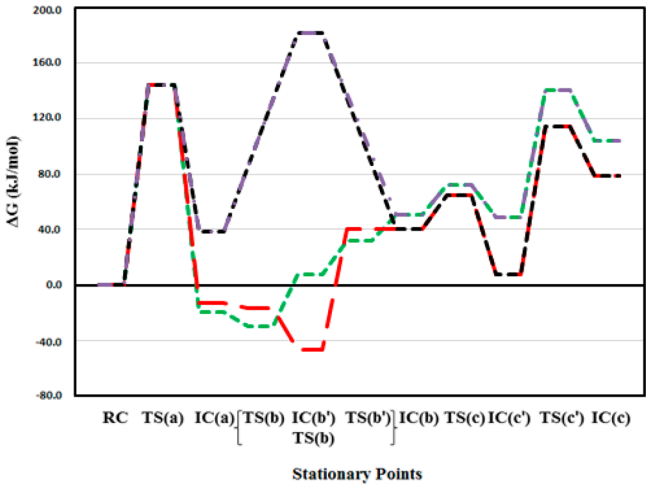

Figure 2. SMD-M06-2*X*/6-311+G(2df,2p)//PCM-B3LYP/6-31G(d) relative Gibbs energies (kJ/mol) for the deglycosylation and β-lyase pathways considered with respect to the *anti* dOG reactant, including N-base assisted ring-opening followed by N-base 3′-phosphate elimination (red, long dashed), O-base assisted ring-opening followed by 3′-phosphate elimination facilitated by O8 of OG (green, short dashed), direct ring-opening followed by O-base 3′-phosphate elimination (purple, dot and dashed), and direct ring-opening followed by N-base 3′-phosphate elimination (black, short dashed).

bacteria, leads to an *anti* dOG conformational preference.[43] Therefore, it appears that the *anti* conformer is more generally preferred. Nevertheless, the present study considers the deglycosylation reaction for both starting dOG conformations (Figure 3). Interestingly, there is good agreement between our calculated *syn* reactant complex and crystal structures corresponding to dOG (PDB ID: 1R2Y)[11] or an abasic site

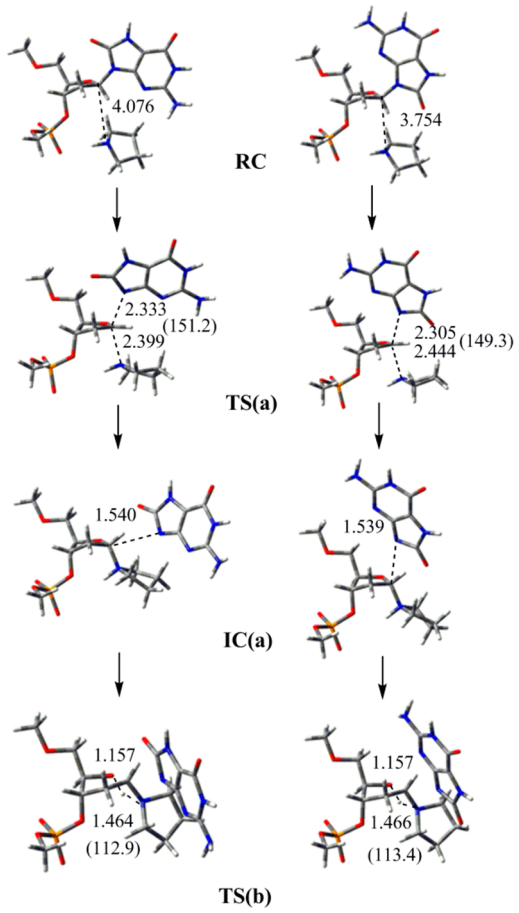

Figure 3. Structures along the deglycosylation (RC, TS(a) and IC(a)) and direct ring-opening (TS(b)) steps initiated from the *anti* (left) and *syn* (right) dOG conformers. Important distances (Å) and angles (deg., in parentheses) obtained at the PCM-B3LYP/6-31G(d) level of theory are provided. The sodium counterion is omitted for clarity.

(PDB ID: 3TWM)[67] bound in the enzyme active site (Figure 4), which lends confidence to our computational approach.

Both calculated reactants (RC, Figure 3) possess C3′-*exo* sugar puckering, and the model proline is positioned on the opposite side of the sugar with respect to the nucleobase and O5′. The reaction proceeds via an S_N2 mechanism, while a parallel S_N1-type reaction could not be identified. The transition states for this step (TS(a), Figure 3) have a

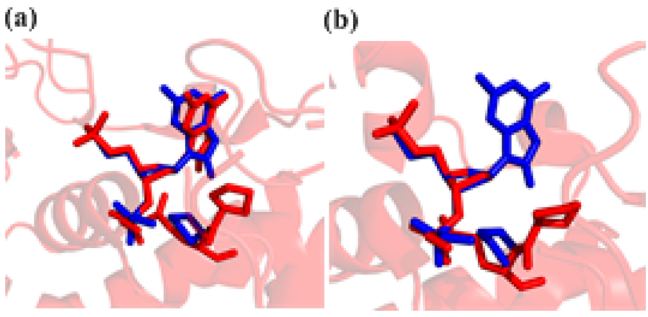

Figure 4. Overlay of the *syn* reactant complex calculated in the present work (blue) with experimental crystal structures corresponding to (a) dOG bound in the active site (PDB ID: 1R2Y) or (b) an abasic-site bound in the active site (PDB ID: 3TWM). Hydrogen atoms and the DNA backbone are not shown for clarity.

dx.doi.org/10.1021/jp507783d | J. Phys. Chem. B 2014, 118, 14566−14577

(breaking) glycosidic bond length of 2.333 or 2.305 Å and a C1′···Nα distance of 2.399 or 2.444 Å for the *anti* or *syn* conformer, respectively. Therefore, the TS occurs slightly earlier for the *syn* conformer. Nevertheless, the ∠(Nα···C1′···N9) angle is similar in the two TSs, being 151.2° for the *anti* and 149.3° for the *syn* conformer. The structural differences lead to energetic differences (Table 1 and Figure 2), where the deglycosylation barrier for the *anti* conformer (148.6 kJ/mol) is slightly larger than that for *syn* dOG (140.2 kJ/mol). Furthermore, the *syn* reactant is 4.0 kJ/mol higher in energy than the *anti* reactant, and the *syn* intermediate for the deglycosylation reaction (IC(a), Figure 3) is 11.5 kJ/mol more stable.

It has been suggested that enzymatic deglycosylation of purine nucleosides can be acid-catalyzed.[68] Therefore, in order to investigate the effect of nucleobase activation prior to deglycosylation, OG was protonated at available donor sites, namely, N3, O6, or O8. Protonation of the nucleobase at N3, O6, or O8 lowers the deglycosylation barrier of the *anti* conformer to 104.6, 102.1, or 69.8 kJ/mol, respectively. Moreover, the corresponding intermediate of this step falls at −27.6, −42.2, or −73.0 kJ/mol, and these intermediates are more stable than the corresponding neutral forms (Table 1). The barrier for the *syn* conformer protonated at O6 or O8 (100.3 and 59.0 kJ/mol, respectively) is even smaller. However, efforts to locate the deglycosylation TS associated with protonated N3 of the *syn* conformer were not successful. Regardless, in agreement with previous studies,[68] activation of the nucleobase through protonation prior to deglycosylation is one way the enzyme can significantly catalyze the reaction. However, since the excised OG must play the role of the general base and acid in several subsequent reaction steps in the present work, neutral OG is implemented throughout to characterize the remainder of the mechanistic pathway.

Ring-Opening. *Direct Proton Transfer.* The ring-opening pathway can occur via direct proton transfer from Nα of the model proline to O4′ of deoxyribose, which can be initiated from the *anti* or *syn* conformer. The intermediates corresponding to the direct pathway (IC(a)) are directly connected to the deglycosylation transition states (Figure 3). Regardless of the starting dOG conformation, this reaction requires significant bending of the proline linkage with respect to the sugar moiety (IC(a) → TS(b), Figure 3). As a result, the geometrical parameters for the reaction core of the associated transition states are nearly identical for both (*anti*/*syn*) dOG conformers. Specifically, the distance between the proton and O4′ is the same (1.157 Å), and *d*(Nα···H) deviates by only 0.002 Å for the *anti* and *syn* pathways. TS(b) falls 180.8 or 178.7 kJ/mol above the overall reactants and $\Delta G^{\ddagger}$ is 143.9 or 153.3 kJ/mol for the *anti* or *syn* orientation, respectively (Table 1 and Figure 2). These significant barriers suggest that there may be an alternative mechanism for the ring-opening step that yields a lower barrier.

Base-Assisted Proton Transfer. Previous work on the dOG glycosylase and β-lyase reaction catalyzed by hOgg1 indicates that a base-assisted proton transfer mechanism can lower the ring-opening barrier.[29] In this pathway (Figure 5), a two-step mechanism is considered in which OG abstracts the proton from Nα in the first step and the proton is delivered from OG to O4′ in the second step (Scheme 2). Consistent with the previous study on hOgg1 bifunctional activity,[29] either O8 or N9 of the excised OG can act as the general base, and the corresponding pathways are denoted as O-base and N-base,

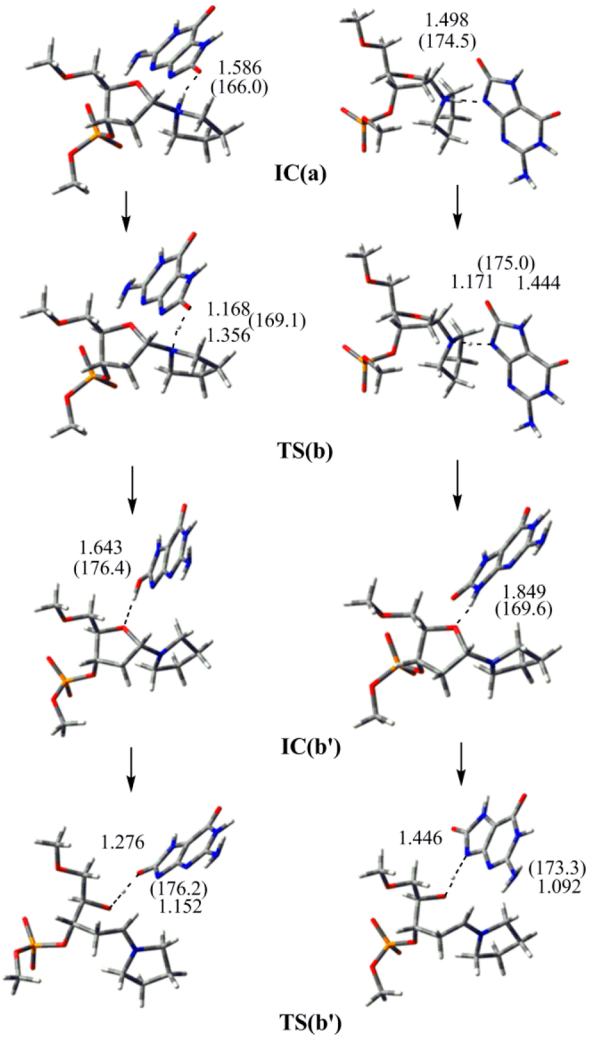

Figure 5. Structures along the assisted ring-opening step (IC(a), TS(b), IC(b′), and TS(b′)) with protonation facilitated by O8 (O-base, left) and N9 (N-base, right) of dOG. Important distances (Å) and angles (deg, in parentheses) obtained at the PCM-B3LYP/6-31G(d) level of theory are provided. The sodium counterion is omitted for clarity.

respectively (Figure 5). However, since proline has only one proton at Nα, either OG must move from the O5′ to the O3′ side of the sugar or the proline linkage must flip to direct the proton toward OG in order for proton abstraction to occur. When OG moves to the O3′ side of the sugar, only O8 can capture the proton from the linkage since steric constraints prevent close contact between N9 of OG and the Nα−H of proline. Alternatively, when the proline flips, a TS could not be identified for proton abstraction by O8.

In addition to the intermediates (IC(a), Figure 3) associated with direct proton transfer, the deglycosylation transition states (TS(a), Figure 3) are connected to two intermediates corresponding to the base-assisted ring-opening pathway (IC(a), Figure 5). The intermediates along the assisted pathways are considerably more stable than those for the direct mechanism (−44.9 kJ/mol for O-base and −11.5 kJ/mol for N-base assisted (Figure 5) compared to 36.9 and 25.4 kJ/mol for *anti* and *syn* direct (Figure 3) ring-opening pathways, respectively). From these intermediates, TS(b) for the assisted mechanism has different geometrical features for the two OG

dx.doi.org/10.1021/jp507783d | J. Phys. Chem. B 2014, 118, 14566−14577

base pathways. Specifically, the C1′···H distance is 1.356 Å for O-base, but only 1.171 Å for N-base. On the other hand, the N9···H distance (1.444 Å) is larger than O8···H (1.168 Å). The proton transfer from Nα to OG is barrierless. In the case of the N-base pathway, the IC(b′) product is the most stable intermediate over the entire reaction pathway (Figure 5). However, this structure is artificially stabilized through interactions between the excised OG and the sodium ion complexed to the C3′ phosphate, which would not occur in the enzymatic environment. The corresponding O-base intermediate lies ∼12 kJ/mol above the reactants.

The second step in the assisted ring-opening pathway is delivery of the proton captured by OG to O4′. In the TSs (TS(b′), Figure 5), *d*(N9···H) (1.446 Å) is longer than *d*(O8···H) (1.276 Å), and *d*(O4′···H) is shorter for the N-base (1.092 Å) than the O-base (1.152 Å) pathway, which follows the trend for the proton abstraction step. In the N-base pathway, there is a weak (2.415 Å) C1′−H···N3 hydrogen-bonding interaction, while there is a slightly stronger C1′−H···N9 interaction (2.228 Å) in the O-base pathway. Interestingly, N9 abstracts (∠(Nα···H···N9)) and delivers (∠(O4′···H···N9)) the proton at a similar angle (deviation less than 2°, Figure 5). On the other hand, the abstraction and the delivery angles for O8 differ by ∼7°. Although Δ*G* of the proton delivery is similar for the O-base and N-base mechanisms (35.6 and 39.9 kJ/mol respectively), the stability of IC(b′) for the N-base pathway leads to a considerable $\Delta G^{\ddagger}$ (98.8 kJ/mol) compared to O-base pathway ($\Delta G^{\ddagger}$ = 23.9 kJ/mol, Table 1 and Figure 2). Since the imine linkage produced in this reaction step is flexible,[29] the IC(b) intermediates (Figure 6) will be taken as the products of both the direct and assisted pathways in order to consider the next (*β*-elimination) reaction step.

Overlays of our calculated ring-opened Schiff base intermediate (IC(b) for the O-base or N-base pathway, Figure 6) and crystal structures corresponding to a borohydride-trapped abasic site complex (PDB ID: 1L1Z)[10] or a Schiff base intermediate (PDB ID: 1K82)[39] are provided in Figure 7. Differences in the calculated structures and 1K82 mainly arise in the ∠(C_{δ}−N−C1′) angle, which is smaller in the constrained crystal (100.1°) than fully optimized structures (123.3° and 126.1° for O-base and N-base intermediates, respectively). Moreover, the calculated *d*(N−C1′) bond length is shorter (1.286 and 1.290 Å for O-base and N-base intermediates, respectively) than that in the crystal structure (1.392 Å), which is indicative of greater sp^2 character of the Schiff base in the fully optimized geometry. On the other hand, the sp^3 hybridization of C1′ in the reduced abasic site intermediate (PDB ID: 1L1Z) leads to larger deviations compared to the calculated Schiff base intermediate (Figure 7). Indeed, the ∠(N−C1′−C2′) angle suggests the experimental structure is nearly tetrahedral at C1′ (111.6°) compared to the sp^2 character in the optimized structures (125.0° and 124.3° for O-base and N-base intermediates, respectively). The observed N−C1′ bond length (1.474 Å) further supports the sp^3 nature of C1′ in 1L1Z. Despite these deviations, our small model fits within crystal structures that mimic different stages of the reaction and thereby recovers important structural features of the cross-link that will be useful in large-scale DNA−protein modeling.

***β*-Elimination.** The third phase of the overall process facilitated by FPG is *β*-elimination (Schemes 1 and 2), which consists of proton abstraction from C2′ followed by O3′ elimination. Similar to the proton abstraction in the assisted

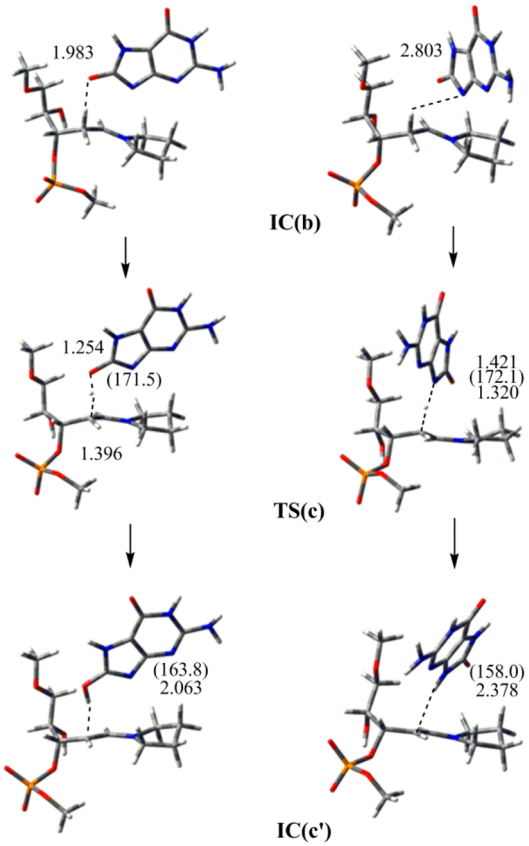

Figure 6. Structures along the proton abstraction step prior to *β*-elimination (IC(b), TS(c) and IC(c′)) facilitated by O8 (O-base, left) and N9 (N-base, right) of dOG. Important distances (Å) and angles (deg, in parentheses) obtained at the PCM-B3LYP/6-31G(d) level of theory are provided. Sodium counterion is omitted for clarity.

ring-opening step, the *β*-elimination step can be facilitated by either O8 or N9 of the excised OG, denoted as the O-base and N-base pathway, respectively. In this step, either the *Pro*-R or *Pro*-S proton may be abstracted; however, since *Pro*-R abstraction requires overcoming a larger barrier due to necessary torsion in the C1′−C2′−C3′ angle,[23,29,32] only *Pro*-S abstraction is considered in this study.

The reaction occurs via an E1cB mechanism within the constraints of the model implemented. The E1cB elimination proceeds through a carbanion intermediate (IC(c′), Figure 6) since Nα of the proline−sugar linkage stabilizes the negative charge developing on C2′ upon proton abstraction. This partial stabilization likely prevents the E2 mechanism. Despite the fact that the potential carbocation intermediate formed along an E1 pathway may be partially stabilized by the imine linkage, the E1 elimination reaction is improbable due to the absence of a strong acid and good leaving group.

In the transition states corresponding to proton abstraction (TS(c), Figure 6), *d*(H···N9) (1.421 Å) is longer than *d*(H···O8) (1.254 Å), which is similar to the proton abstraction in the assisted ring-opening step (TS(b), Figure 5). However, *d*(C2′···H) is shorter for N-base than O-base, which is opposite the situation for TS(b). $\Delta G^{\ddagger}$ for TS(c) is 15.0 kJ/mol larger for N-base than O-base with respect to the corresponding reactants IC(b). However, since the intermediate IC(b) is more stable for N-base, the corresponding $\Delta G^{\ddagger}$ is 14.0 kJ/mol larger.

Proton abstraction is followed by O3′ elimination. In the transition states (TS(c′), Figure 8), the *d*(C3′···O3′) distance is

dx.doi.org/10.1021/jp507783d | J. Phys. Chem. B 2014, 118, 14566−14577

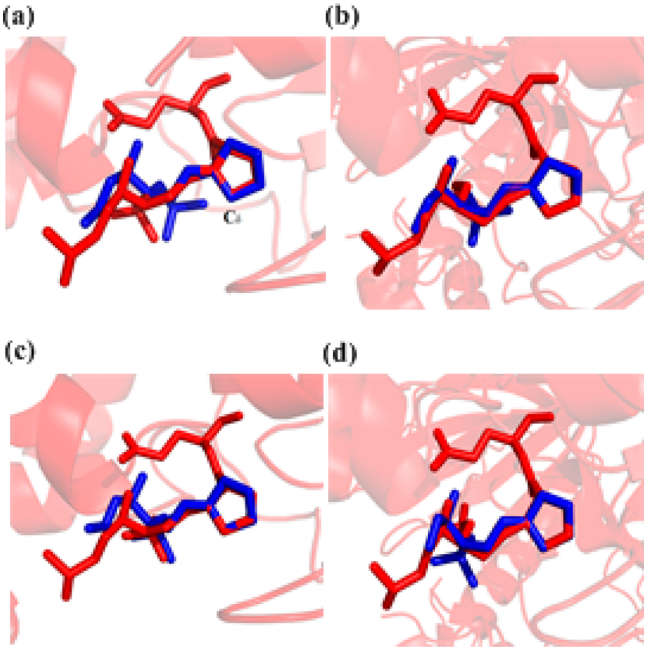

Figure 7. Overlay of the ring-opened Schiff base (IC(b)) calculated in the present work (blue) for the O-base (a and b) or N-base (c and d) pathway with crystal structures corresponding to a Schiff base intermediate (a and c; PDB ID: 1L1Z) or a borohydride-trapped abasic-site complex (b and d; PDB ID: 1K82). Hydrogen atoms and DNA backbone are not shown for clarity.

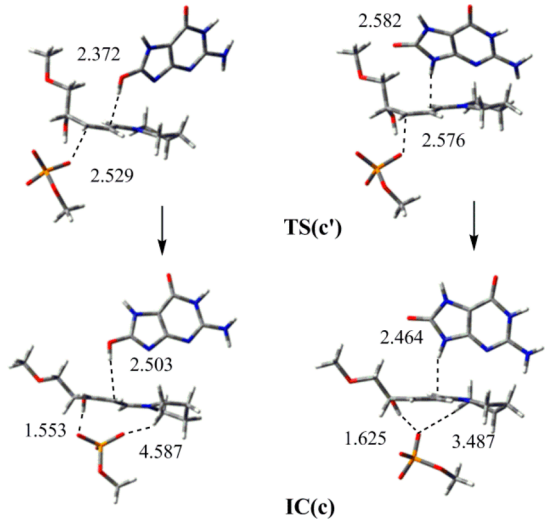

Figure 8. Structures along the elimination step (TS(c′) and IC(c)) associated with the O-base (left) and N-base (right) pathways. Important distances (Å) and angles (deg, in parentheses) obtained at the PCM-B3LYP/6-31G(d) level of theory are provided. The sodium counterion is omitted for clarity.

2.529 or 2.576 Å for the O-base or N-base pathway, respectively. In the final elimination products (IC(c), Figure 8), d(C2′···H) is 2.503 Å to O8 and 2.464 Å to N9, which are longer and shorter than in the corresponding TSs, respectively. Hydrogen-bonding interactions between the oxygen of the excised phosphate group and O4′−H stabilize the elimination products. However, the mobility of the phosphate group toward O4′−H arises from the truncated model used in the present work, and the final products of the enzymatic reaction may be significantly different.

DISCUSSION

Although an abundance of experimental and computational work has shed light on many aspects of the mechanism of action of hOgg1,[14,22,24−26,29,36,58] only one computational study has considered the chemical steps involved in the bifunctional activity of FPG.[46] Furthermore, little experimental evidence is available for the details of each phase of the FPG reaction. Since hOgg1 and FPG differ in the nucleophile,[31,32] active site residues,[31,32] lesion specificity,[31−36] possible activity modes,[16,18−23] and efficiency,[10,38] extension of previous computational studies on hOgg1 to FPG may not be possible. Therefore, the present work completed the first computational study of the chemical steps associated with the glycosylase and β-lyase activity of FPG (Schemes 1 and 2). By using the same approaches as implemented in a previous study on hOgg1,[29] an accurate comparison between the intrinsic chemistry facilitated by FPG and hOgg1 is obtained that provides information about the preferred reaction pathways and the associated energetic barriers, as well as potential roles for active sites residues. This work thereby provides clues about the influence of the nucleophile on the relative efficiencies and specificities of these enzymes. To this end, each phase of the FPG catalyzed reaction will be separately discussed below, while drawing important comparisons to hOgg1.

Deglycosylation. Excision of the damaged nucleobase is the first step catalyzed by FPG during the BER pathway. Experimental data supports different mechanisms for this step.[10,11] Specifically, Pro2 has been proposed to be perfectly positioned for (S_N2) attack on C1′,[10] while another study indicates that Pro2 lies close to C1′, but is not well aligned for an S_N2-type reaction.[11] In agreement with a previous computational study on the FPG[46] and hOgg1[29] glycosylase activity, the model implemented in the current work only resulted in an S_N2 deglycosylation pathway. Interestingly, the deglycosylation transition state occurs later when proline acts as the nucleophile rather than lysine,[29] where the d(Nα···C1′) distances in the transition state for *anti* dOG deglycosylation are similar (only 0.018 Å longer for proline), while the d(C1′··· N9) distance is (0.108 Å) shorter for proline.

Previous studies suggest that dOG can adopt either the *anti* or *syn* conformation in the FPG recognition pocket, with the *anti* conformer being more favorable.[44,45] Therefore, we considered deglycosylation initiated from either dOG conformer. The *anti* dOG transition state occurs later than the *syn* variant, with d(Nα···C1′) being 0.065 Å longer and d(C1′··· N9) being 0.028 Å shorter for *anti* dOG. Furthermore, although the *syn* conformer lies 4.0 kJ/mol above the *anti* conformer, the *syn* deglycosylation barrier is 8.4 kJ/mol smaller than that for the *anti* orientation. This suggests that *syn* dOG is the intrinsically most favored conformer for excision. Nevertheless, interactions between dOG and the enzyme may affect these relatively small calculated energy differences.

The deglycosylation barriers for the *anti* (148.6 kJ/mol) and *syn* (140.2 kJ/mol) dOG conformers using proline are similar to those for lysine calculated with the same level of theory (147.4 kJ/mol),[29] as well as other computational investigations.[25,26,28,29] Thus, our calculations predict that deglycosylation is the rate-determining step (for the most favorable, assisted ring-opening pathway). However, experimental studies have determined that the lyase step is the overall rate-limiting step in the BER chemical process.[18,69] Thus, consistent with other glycosylases,[70,71] including hOgg1,[29] FPG must signifi-

dx.doi.org/10.1021/jp507783d | J. Phys. Chem. B 2014, 118, 14566−14577

cantly reduce the deglycosylation barrier. The hOgg1 catalyzed deglycosylation has been previously proposed to be facilitated by OG hydrogen bonding with (or being protonated via) active site water or amino acids.[12,16,58,72−75] Indeed, our model indicates that *anti* dOG protonation significantly reduces the deglycosylation barrier (by 50−80 kJ/mol depending on the OG site used for abstraction) and produces a more stable intermediate (by 55−105 kJ/mol). Unfortunately, however, no residue capable of protonating OG at O6 can be found in the experimental X-ray structure (1R2Y) of the enzyme−substrate complex[46] (Figure 9). Nevertheless, at least partial activation of

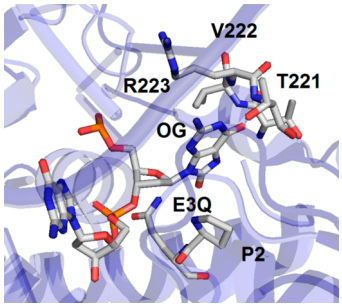

Figure 9. Important FPG active site residues identified in the crystal structure of the E3Q mutant (PDB ID: 1R2Y).[11]

OG may occur through hydrogen-bonding interactions between O6 of OG and Thr221, Val222, Arg223 and Thr224[11] (Figure 7). Alternatively, it has been proposed that Glu2 could protonate OG at the O8 position[11,68] (Figure 7), which may be possible depending on the protonation state upon binding.

We anticipate that including any of these residues in a larger computational model will lower the calculated deglycosylation barrier through, for example, partial protonation of the departing base via hydrogen-bonding interactions. In fact, it has been previously shown that hydrogen-bonding interactions can significantly affect the acidity of the canonical and damaged nucleobases,[76,77] including OG, and therefore decrease the deglycosylation barrier.[78] Hence, we anticipate that partial protonation will lead to a barrier height between those calculated in the present study for the neutral and fully protonated dOG deglycosylation pathways.

In addition to nucleobase activation, the catalytically important Asp268 has been proposed to stabilize the positive charge accumulating on the DNA−protein cross-link in the deglycosylation step catalyzed by hOgg1.[15,16] If Glu2 is anionic upon binding or transfers a proton to O6 of OG upon base departure, then Glu2 may stabilize the positive charge forming at this point along the FPG catalyzed reaction. This proposal is supported by the fact that there is a short distance between Glu2 (or the mutant Gln2) and O4′ (3.1 to 3.4 Å) in many crystal structures.[10,11,40,79] Furthermore, electrostatic stabilization is a role commonly assigned to Asp/Glu residues positioned near the sugar in the active site of most DNA glycosylases (see, for example, refs 15, 39, and 67).

Ring-Opening. The ring-opening step (Scheme 1 and 2) differs from the previously considered lysine-catalyzed reaction since there is only one proton transfer possibility from Nα of proline (compared to two protons on Nε of lysine). Transfer of the Nα proton either directly or via a general base was considered in the present work. Direct proton transfer from Nα to O4′ coupled with ring-opening was initiated from either the *anti* (Figure 3, right) or *syn* (Figure 3, left) orientation of the excised OG relative to the sugar. Although key geometrical features (i.e., d(O4′···H) and d(Nα···H)) are nearly identical for the two reaction pathways (deviate by less than 0.002 Å), the corresponding distances are shorter for the (*anti*) lysine reaction (by 0.039 and 0.048 Å, respectively).[29] Nevertheless, as found for the lysine nucleophile,[29] the barriers for direct proton transfer from cross-linked proline (∼140 to 150 kJ/mol) are high due to the significant torsion required on the Nα−C1′ bond. Therefore, proton transfer facilitated by the excised OG was considered, which significantly reduces the ring-opening barrier (by ∼115 kJ/mol for abstraction facilitated by O8 of OG). In fact, in agreement with the previous study on lysine,[29] the base-assisted proton transfer is barrierless (by up to approximately −10 kJ/mol; Table 1 and Figure 2). Although proton delivery from OG to O4′ necessitates overcoming a barrier of ∼25 kJ/mol (for the more favorable O-base pathway), this is much less than the favored direct proton transfer barrier.

The barrierless proton abstraction from Nα indicates that the cross-link easily delivers the proton to moieties in the proximity of the linkage. Because the Nα proton and departed OG are on opposite sides of the sugar moiety, proton transfer to OG is unlikely in the enzyme. Nevertheless, proton delivery to O4′ may be facilitated by a different active site residue in FPG. In fact, the predicted ease of the proton delivery supports proposed proton transfer from the cross-linked Nα to Glu3 through a tight hydrogen-bonding network of crystallographic water molecules,[32] which would then allow Glu3 to protonate O4′. The proposal that Glu3 acts as the general acid is further supported by evidence that O4′ of the sugar moiety forms a strong hydrogen bond to Oα2 of Glu3,[32] and that Glu3 is in close proximity of O4′ in most crystal structures.[10,11,40,79]

The previous computational study on hOgg1 glycosylase and β-lyase activity[29] identified the lowest energy point on the PES as the DNA−protein cross-link after lysine is deprotonated, but before the ring-opening step. This novel finding was the first computational support for the observed dissociation of hOgg1 from the abasic site by the human AP Endonuclease (APE1, EC#: 4.2.99.18) prior to the β-elimination step,[16,18,19,21,22] and monofunctional activity of hOgg1 *in vivo*.[18−23] In the present work, the equivalent point on the PES (without artificial stabilization due to the computational model) for FPG glycosylase and β-lyase activity lies ∼12 kJ/mol above the reactants. Therefore, unlike the case of hOgg1, the current work does not strongly support a monofunctional activity mode for FPG, which may explain the lack of experimental evidence for FPG monofunctional activity. Furthermore, the potential absence of analogous monofunctional activity may rationalize the greater efficiency, as well as unique δ-lyase activity, for FPG over hOgg1.

β-Elimination. Although one experimental study suggests that OG diffuses out of the active site after glycosidic bond cleavage,[10] OG has been proposed to be involve in the C2′−H abstraction step.[12,58] Alternatively, although a crystallographic water molecule has been implicated in this step,[10] the water does not hydrogen bond with the protein, and is not observed in the related *E. coli* FPG and Nei enzymes.[32] Thus, the identity of the general base for the C2′−H abstraction step is currently unclear. As a result, two pathways were characterized for the elimination step in the present work, which begin with C2′−H abstraction by OG as the general base. The proton abstraction

dx.doi.org/10.1021/jp507783d | J. Phys. Chem. B 2014, 118, 14566−14577

occurs with a relatively small barrier (approximately 20−35 kJ/mol depending on the OG site involved, Table 1).

The elimination step is complete when the 3′-phosphate dissociates. As for lysine,[29] this step occurs through an E1cB mechanism, which involves a carbanion intermediate that is stabilized by the positive charge on the cross-linked proline. In the transition state, the key O3′···C3′ distance is similar for proline and lysine nucleophile,[29] and therefore changes in the Gibbs free energy for the elimination step range from approximately 100−135 kJ/mol regardless of the (O-base or N-base) pathway or nucleophile (proline or lysine).[29] Although the elimination barrier is slightly lower than the deglycosylation and direct ring-opening barriers, the presence of a sodium cation in our model artificially reduces the core barrier compared to an isolated phosphate group. Therefore, the phosphate group must be activated for departure in the enzyme. In FPG, this may be accomplished through interactions between the 3′-phosphate and conserved Lys56, Asn168, and Arg258 residues.[39] Interestingly, this role was proposed to be filled by a calcium dication in the active site and/or the solvent exposure of the phosphate moiety in hOgg1.[29] The importance of this stabilization predicted by our calculations coupled with the greater anticipated stabilization provided by FPG provides additional clues regarding the greater efficiency, and lack of observed monofunctional activity, for FPG.

CONCLUSION

For the first time, the present work uses the smallest computational model feasible (modified nucleoside-3′-monophosphate with a truncated proline nucleophile) to fully explore possible pathways for the bifunctional activity of bacterial FPG, which removes 8-oxoguanine from DNA. The overall process was divided into three main phases, namely, deglycosylation, (deoxyribose) ring-opening, and β-elimination, and unique findings were obtained about each step that help explain how this important enzyme can facilitate this seemingly difficult chemistry. Specifically, our calculations indicate that the deglycosylation barrier must be significantly reduced by the protein. Available crystal structures suggest this may be achieved by stabilizing the departing (anionic) OG (through protonation or a network of active site hydrogen-bonding interactions) and the positive charge developing on the DNA−protein cross-link (through interactions with a Glu side chain positioned near the deoxyribose moiety, which is similar to the role proposed for Asp/Glu in many other glycosylases). Although direct proton transfer from Nα of the cross-linked proline to O4′ of the sugar moiety requires overcoming a significant barrier in the second (ring-opening) phase, proton transfer assisted by a general base and acid is extremely favorable, which may be achieved in the enzyme through a hydrogen-bonding network of crystallographic water. Although the barrier for the final (elimination) step is less than those of the deglycosylation and direct ring-opening phases, considerable energy is still required and therefore the enzyme must also catalyze this step. Indeed, several FPG active site residues (including Lys, Arg and Asn side chains) interact with the 3′-phosphate group and may provide this critical stabilization.

The key conclusions from our study on FPG glycosylase and β-lyase activity parallel those from a previous study on the corresponding human enzyme (hOgg1) using a similar computational model. This suggests that the majority of differences between hOgg1 and FPG bifunctional activity do not arise due to differences in the intrinsic chemistry of the nucleophile, but rather deviations in other active site residues. For example, base departure is facilitated by different species in each enzyme due to the unique composition of each active site, which explains the distinct substrate specificity of each enzyme. Furthermore, the β-elimination step is facilitated by several tight hydrogen-bonding interactions in FPG, while a calcium dication is near the solvent-exposed 3′-phosphate when bound to hOgg1, which in part justifies the greater efficiency of FPG over hOgg1. Nevertheless, the nucleophile implemented may rationalize why monofunctional activity has been reported for hOgg1, but not FPG, in vivo. Specifically, only the lysine nucleophile stabilizes a low energy intermediate along the reaction pathway that can be hydrolyzed to afford monofunctional activity. These conclusions based on our models and careful analysis of available crystal structures must be verified with future large-scale modeling of the favorable pathways identified in the present work for these two key BER enzymes.

ASSOCIATED CONTENT

Supporting Information

Full citations for refs 9 and 59, and Cartesian coordinates for all transition states. This material is available free of charge via the Internet at http://pubs.acs.org.

AUTHOR INFORMATION

Corresponding Author

*E-mail: stacey.wetmore@uleth.ca. Phone: 1 403 329 2323.

Notes

The authors declare no competing financial interest.

ACKNOWLEDGMENTS

Financial support was provided by the Natural Sciences and Engineering Council of Canada (NSERC), the Canada Research Chair program, and the Canada Foundation for Innovation (CFI). Computer resources were provided by NUCLEIC (New Upscale Cluster for Lethbridge to Enable Innovative Chemistry) and WestGrid, part of the Compute/Calcul Canada HPC platform.

REFERENCES

(1) Barnett, R. N.; Bongiorno, A.; Cleveland, C. L.; Joy, A.; Landman, U.; Schuster, G. B. Oxidative Damage to DNA: Counterion-Assisted Addition of Water to Ionized DNA. *J. Am. Chem. Soc.* **2006**, *128*, 10795−10800.

(2) Kamiya, H. Mutagenic Potentials of Damaged Nucleic Acids Produced by Reactive Oxygen/Nitrogen Species: Approaches Using Synthetic Oligonucleotides and Nucleotides. *Nucleic Acids Res.* **2003**, *31*, 517−531.

(3) Cadet, J.; Douki, T.; Ravanat, J.-L. Oxidatively Generated Base Damage to Cellular DNA. *Free Radical Biol. Med.* **2010**, *49*, 9−21.

(4) Kanvah, S.; Joseph, J.; Schuster, G. B.; Barnett, R. N.; Cleveland, C. L.; Landman, U. Oxidation of DNA: Damage to Nucleobases. *Acc. Chem. Res.* **2010**, *43*, 280−287.

(5) van Loon, B.; Markkanen, E.; Hübscher, U. Oxygen as a Friend and Enemy: How to Combat the Mutational Potential of 8-Oxoguanine. *DNA Repair* **2010**, *9*, 604−616.

(6) Sakai, A.; Nakanishi, M.; Yoshiyama, K.; Maki, H. Impact of Reactive Oxygen Species on Spontaneous Mutagenesis in *Escherichia coli*. *Genes to Cells* **2006**, *11*, 767−778.

(7) Fujimoto, H.; Pinak, M.; Nemoto, T.; Bunta, J. K. Structural Analysis of Base Mispairing in DNA Containing Oxidative Guanine Lesion. *Cent. Eur. J. Phys.* **2007**, *5*, 49−61.

(8) McCulloch, S. D.; Kokoska, R. J.; Garg, P.; Burgers, P. M.; Kunkel, T. A. The Efficiency and Fidelity of 8-Oxo-guanine Bypass by DNA Polymerases δ and η. *Nucleic Acids Res.* **2009**, *37*, 2830−2840.
(9) Greenman, C.; Stephens, P.; Smith, R.; Dalgliesh, G. L.; Hunter, C.; Bignell, G.; Davies, H.; Teague, J.; Butler, A.; Edkins, S.; et al. Patterns of Somatic Mutation in Human Cancer Genomes. *Nature (London, U. K.)* **2007**, *446*, 153−158.
(10) Fromme, J. C.; Verdine, G. L. Structural Insights into Lesion Recognition and Repair by the Bacterial 8-Oxoguanine DNA Glycosylase MutM. *Nat. Struct. Biol.* **2002**, *9*, 544−552.
(11) Fromme, J. C.; Verdine, G. L. DNA Lesion Recognition by the Bacterial Repair Enzyme MutM. *J. Biol. Chem.* **2003**, *278*, 51543−51548.
(12) Fromme, J. C.; Bruner, S. D.; Yang, W.; Karplus, M.; Verdine, G. L. Product-Assisted Catalysis in Base-Excision DNA Repair. *Nat. Struct. Biol.* **2003**, *10*, 204−211.
(13) McCullough, A. K.; Dodson, M. L.; Lloyd, R. S. Initiation of Base Excision Repair: Glycosylase Mechanisms and Structures. *Annu. Rev. Biochem.* **1999**, *68*, 255−285.
(14) Nash, H. M.; Lu, R. Z.; Lane, W. S.; Verdine, G. L. The Critical Active-Site Amine of the Human 8-Oxoguanine DNA Glycosylase, hOgg1: Direct Identification, Ablation and Chemical Reconstitution. *Chem. Biol.* **1997**, *4*, 693−702.
(15) Norman, D. P. G.; Chung, S. J.; Verdine, G. L. Structural and Biochemical Exploration of a Critical Amino Acid in Human 8-Oxoguanine Glycosylase. *Biochemistry* **2003**, *42*, 1564−1572.
(16) Dalhus, B.; Forsbring, M.; Helle, I. H.; Vik, E. S.; Forstrøm, R. J.; Backe, P. H.; Alseth, I.; Bjørås, M. Separation-of-Function Mutants Unravel the Dual-Reaction Mode of Human 8-Oxoguanine DNA Glycosylase. *Structure (Cambridge, MA, U. S.)* **2011**, *19*, 117−127.
(17) Sung, R. J.; Zhang, M.; Qi, Y.; Verdine, G. L. Structural and Biochemical Analysis of DNA Helix Invasion by the Bacterial 8-Oxoguanine DNA Glycosylase MutM. *J. Biol. Chem.* **2013**, *288*, 10012−10023.
(18) Zharkov, D. O.; Rosenquist, T. A.; Gerchman, S. E.; Grollman, A. P. Substrate Specificity and Reaction Mechanism of Murine 8-Oxoguanine-DNA Glycosylase. *J. Biol. Chem.* **2000**, *275*, 28607−28617.
(19) Hill, J. W.; Hazra, T. K.; Izumi, T.; Mitra, S. Stimulation of Human 8-Oxoguanine-DNA Glycosylase by AP-Endonuclease: Potential Coordination of the Initial Steps in Base Excision Repair. *Nucleic Acids Res.* **2001**, *29*, 430−438.
(20) Kuznetsov, N. A.; Koval, V. V.; Zharkov, D. O.; Nevinsky, G. A.; Douglas, K. T.; Fedorova, O. S. Kinetics of Substrate Recognition and Cleavage by Human 8-Oxoguanine-DNA Glycosylase. *Nucleic Acids Res.* **2005**, *33*, 3919−3931.
(21) Morland, I.; Luna, L.; Gustad, E.; Seeberg, E.; Bjørås, M. Product Inhibition and Magnesium Modulate the Dual Reaction Mode of hOgg1. *DNA Repair* **2005**, *4*, 381−387.
(22) Vidal, A. E.; Hickson, I. D.; Boiteux, S.; Radicella, J. P. Mechanism of Stimulation of the DNA Glycosylase Activity of hOGG1 by the Major Human AP Endonuclease: Bypass of the AP Lyase Activity Step. *Nucleic Acids Res.* **2001**, *29*, 1285−1292.
(23) Sidorenko, V. S.; Grollman, A. P.; Jaruga, P.; Dizdaroglu, M.; Zharkov, D. O. Substrate Specificity and Excision Kinetics of Natural Polymorphic Variants and Phosphomimetic Mutants of Human 8-Oxoguanine-DNA Glycosylase. *FEBS J.* **2009**, *276*, 5149−5162.
(24) Osakabe, T.; Fujii, Y.; Hata, M.; Tsuda, M.; Neya, S.; Hoshino, T. Quantum Chemical Study on Base Excision Mechanism of 8-Oxoguanine DNA Glycosylase: Substrate-Assisted Catalysis of the N-Glycosidic Linkage Cleavage Reaction. *Chem-Bio Inf. J.* **2004**, *4*, 73−92.
(25) Schyman, P.; Danielsson, J.; Pinak, M.; Laaksonen, A. Theoretical Study of the Human DNA Repair Protein hOGG1 Activity. *J. Phys. Chem. A* **2005**, *109*, 1713−1719.
(26) Calvaresi, M.; Bottoni, A.; Garavelli, M. Computational Clues for a New Mechanism in the Glycosylase Activity of the Human DNA Repair Protein hOGG1. A Generalized Paradigm for Purine-Repairing Systems? *J. Phys. Chem. B* **2007**, *111*, 6557−6570.
(27) Zheng, Y.; Xue, Y.; Yan, S. G. The Effects of Oxidation and Protonation on the N-Glycosidic Bond Stability of 8-Oxo-2′-deoxyguanosine: DFT Study. *THEOCHEM* **2008**, *860*, 52−57.
(28) Shim, E. J.; Przybylski, J. L.; Wetmore, S. D. Effects of Nucleophile, Oxidative Damage, and Nucleobase Orientation on the Glycosidic Bond Cleavage in Deoxyguanosine. *J. Phys. Chem. B* **2010**, *114*, 2319−2326.
(29) Kellie, J. L.; Wetmore, S. D. Mechanistic and Conformational Flexibility of the Covalent Linkage Formed During β-Lyase Activity on an AP-Site: Application to hOgg1. *J. Phys. Chem. B* **2012**, *116*, 10786−10797.
(30) Tchou, J.; Bodepudi, V.; Shibutani, S.; Antoshechkin, I.; Miller, J.; Grollman, A. P.; Johnson, F. Substrate Specificity of Fpg Protein. Recognition and Cleavage of Oxidatively Damaged DNA. *J. Biol. Chem.* **1994**, *269*, 15318−15324.
(31) Brooks, S. C.; Adhikary, S.; Rubinson, E. H.; Eichman, B. F. Recent Advances in the Structural Mechanisms of DNA Glycosylases. *Biochim. Biophys. Acta* **2013**, *1*, 247−271.
(32) Zharkov, D. O.; Shoham, G.; Grollman, A. P. Structural Characterization of the Fpg Family of DNA Glycosylases. *DNA Repair* **2003**, *2*, 839−862.
(33) Wiederholt, C. J.; Delaney, M. O.; Pope, M. A.; David, S. S.; Greenberg, M. M. Repair of DNA Containing Fapy·dG and its Beta-C-nucteoside Analogue by Formamidopyrimidine DNA Glycosylase and MutY. *Biochemistry* **2003**, *42*, 9755−9760.
(34) Gasparutto, D.; Muller, E.; Boiteux, S.; Cadet, J. Excision of the Oxidatively Formed 5-Hydroxyhydantoin and 5-Hydroxy-5-methylhydantoin Pyrimidine Lesions by *Escherichia coli* and Saccharomyces Cerevisiae DNA *N*-Glycosylases. *Biochim. Biophys. Acta, Gen. Subj.* **2009**, *1790*, 16−24.
(35) Hatahet, Z.; Kow, Y. W.; Purmal, A. A.; Cunningham, R. P.; Wallace, S. S. New Substrates for Old Enzymes. 5-Hydroxy-2′-deoxycytidine and 5-Hydroxy-2′-deoxyuridine are Substrates for *Escherichia coli* Endonuclease III and Formamidopyrimidine DNA N-glycosylase, while 5-Hydroxy-2′-deoxyuridine is a Substrate for Uracil DNA *N*-Glycosylase. *J. Biol. Chem.* **1994**, *269*, 18814−18820.
(36) Tchou, J.; Kasai, H.; Shibutani, S.; Chung, M. H.; Laval, J.; Grollman, A. P.; Nishimura, S. 8-Oxoguanine (8-Hydroxyguanine) DNA Glycosylase and Its Substrate-Specificity. *Proc. Natl. Acad. Sci. U. S. A.* **1991**, *88*, 4690−4694.
(37) Bhagwat, M.; Gerlt, J. A. 3′- and 5′-Strand Cleavage Reactions Catalyzed by the Fpg Protein from *Escherichia coli* Occur via Successive β- and δ-Elimination Mechanisms, Respectively. *Biochemistry* **1996**, *35*, 659−665.
(38) Frosina, G. Gene Prophylaxis by a DNA Repair Function. *Mol. Aspects Med.* **2007**, *28*, 323−344.
(39) Gilboa, R.; Zharkov, D. O.; Golan, G.; Fernandes, A. S.; Gerchman, S. E.; Matz, E.; Kycia, J. H.; Grollman, A. P.; Shoham, G. Structure of Formamidopyrimidine-DNA Glycosylase Covalently Complexed to DNA. *J. Biol. Chem.* **2002**, *277*, 19811−19816.
(40) Coste, F.; Ober, M.; Carell, T.; Boiteux, S.; Zelwer, C.; Castaing, B. Structural Basis for the Recognition of the FapydG Lesion (2,6-Diamino-4-hydroxy-5-formamidopyrimidine) by Formamidopyrimidine-DNA Glycosylase. *J. Biol. Chem.* **2004**, *279*, 44074−44083.
(41) Pereira de Jesus, K.; S, L.; Zelwer, C.; Castaing, B. Structural Insights into Abasic Site for Fpg Specific Binding and Catalysis: Comparative High-Resolution Crystallographic Studies of Fpg Bound to Various Models of Abasic Site Analogies-Containing DNA. *Nucleic Acids Res.* **2005**, *33*, 5936−5944.
(42) Amara, P.; Serre, L.; Castaing, B.; Thomas, A. Insights into the DNA Repair Process by the Formamidopyrimidine-DNA Glycosylase Investigated by Molecular Dynamics. *Protein Sci.* **2004**, *13*, 2009−2021.
(43) Song, K.; Hornak, V.; Santos, C. D.; Grollman, A. P.; Simmerling, C. Computational Analysis of the Mode of Binding of 8-Oxoguanine to Formamidopyrimidine-DNA Glycosylase. *Biochemistry* **2006**, *45*, 10886−10894.
(44) Perlow-Poehnelt, R. A.; Zharkov, D. O.; Grollman, A. P.; Broyde, S. Substrate Discrimination by Formamidopyrimidine-DNA

Glycosylase: Distinguishing Interactions within the Active Site. *Biochemistry* **2004**, *43*, 16092−16105.
(45) Zaika, E. I.; Perlow, R. A.; Matz, E.; Broyde, S.; Gilboa, R.; Grollman, A. P.; Zharkov, D. O. Substrate Discrimination by Formamidopyrimidine-DNA Glycosylase: A Mutational Analysis. *J. Biol. Chem.* **2004**, *279*, 4849−4861.
(46) Zheng, J. H.; Tan, H. W.; Chen, G. J. Theoretical Study on the Mechanism of the DNA Repair Protein Fpg. *Int. J. Quantum Chem.* **2011**, *111*, 2454−2463.
(47) Frosina, G. Tumor Suppression by DNA Base Excision Repair. *Mini Rev. Med. Chem.* **2007**, *7*, 727−743.
(48) Liu, L.; Nakatsuru, Y.; Gerson, S. L. Base Excision Repair as a Therapeutic Target in Colon Cancer. *Clin. Cancer Res.* **2002**, *8*, 2985−2991.
(49) Madhusudan, S.; Middleton, M. R. The Emerging Role of DNA Repair Proteins as Predictive, Prognostic and Therapeutic Targets in Cancer. *Cancer Treat. Rev.* **2005**, *31*, 603−617.
(50) Damia, G.; D'Incalci, M. Targeting DNA Repair as a Promising Approach in Cancer Therapy. *Eur. J. Cancer* **2007**, *43*, 1791−1801.
(51) Kelley, M. R.; Fishel, M. L. DNA Repair Proteins as Molecular Targets for Cancer Therapeutics. *Anti-Cancer Agents Med. Chem.* **2008**, *8*, 417−425.
(52) Boiteux, S.; O'Connor, T. R.; Laval, J. Formamidopyrimidine-DNA Glycosylase of *Escherichia coli*: Cloning and Sequencing of the Fpg Structural Gene and Overproduction of the Protein. *EMBO J.* **1987**, *6*, 3177−3183.
(53) Rabow, L. E.; Kow, Y. W. Mechanism of Action of Base Release by *Escherichia coli* Fpg Protein: Role of Lysine 155 in Catalysis. *Biochemistry* **1997**, *36*, 5084−5096.
(54) Sidorkina, O. M.; Laval, J. Role of Lysine-57 in the Catalytic Activities of *Escherichia coli* Formamidopyrimidine-DNA Glycosylase (Fpg Protein). *Nucleic Acids Res.* **1998**, *26*, 5351−5357.
(55) Lenz, Stefan A. P.; Kellie, J. L.; Wetmore, S. D. Glycosidic Bond Cleavage in Deoxynucleotides: Effects of Solvent and the DNA Phosphate Backbone in the Computational Model. *J. Phys. Chem. B* **2012**, *116*, 14275−14284.
(56) Millen, A. L.; Manderville, R. A.; Wetmore, S. D. Conformational Flexibility of C8-Phenoxyl-2′-deoxyguanosine Nucleotide Adducts. *J. Phys. Chem. B* **2010**, *114*, 4373−4382.
(57) Churchill, C. D. M.; Wetmore, S. D. Developing a Computational Model that Accurately Reproduces the Structural Features of a Dinucleoside Monophosphate Unit within B-DNA. *Phys. Chem. Chem. Phys.* **2011**, *13*, 16373−16383.
(58) Bruner, S. D.; Norman, D. P. G.; Verdine, G. L. Structural Basis for Recognition and Repair of the Endogenous Mutagen 8-Oxoguanine in DNA. *Nature (London, U. K.)* **2000**, *403*, 859−866.
(59) Frisch, M. J.; Trucks, G. W.; Schlegel, H. B.; Scuseria, G. E.; Robb, M. A.; Cheeseman, J. R.; Scalmani, G.; Barone, V.; Mennucci, B.; Petersson, G. A., et al. *Gaussian 09*, revision C.01; Gaussian, Inc.: Wallingford, CT, 2009.
(60) Zhao, Y.; Truhlar, D. G. Density Functional Calculations of E2 and S(N)2 Reactions: Effects of the Choice of Density Functional, Basis Set, and Self-Consistent Iterations. *J. Chem. Theory Comput.* **2010**, *6*, 1104−1108.
(61) Gilson, M. K.; Honig, B. H. The Dielectric Constant of a Folded Protein. *Biopolymers* **1986**, *25*, 2097−2119.
(62) Nakamura, H.; Sakamoto, T.; Wada, A. A Theoretical Study of the Dielectric Constant of Protein. *Protein Eng.* **1988**, *2*, 177−183.
(63) Karplus, M.; McCammon, J. A. The Internal Dynamics of Globular Proteins. *CRC Crit. Rev. Biochem.* **1981**, *9*, 293−349.
(64) Simonson, T.; Perahia, D.; Bricogne, G. Intramolecular Dielectric Screening in Proteins. *J. Mol. Biol.* **1991**, *218*, 859−886.
(65) Simonson, T.; Perahia, D.; Brunger, A. T. Microscopic Theory of the Dielectric Properties of Proteins. *Biophys. J.* **1991**, *59*, 670−690.
(66) Simonson, T.; Perahia, D. Internal and Interfacial Dielectric Properties of Cytochrome c from Molecular Dynamics in Aqueous Solution. *Proc. Natl. Acad. Sci. U.S.A.* **1995**, *92*, 1082−1086.
(67) Duclos, S.; Aller, P.; Jaruga, P.; Dizdaroglu, M.; Wallace, S. S.; Doublie, S. Structural and Biochemical Studies of a Plant Formamidopyrimidine-DNA Glycosylase Reveal why Eukaryotic Fpg Glycosylases Do Not Excise 8-Oxoguanine. *DNA Repair* **2012**, *11*, 714−725.
(68) Berti, P. J.; McCann, J. A. B. Toward a Detailed Understanding of Base Excision Repair Enzymes: Transition State and Mechanistic Analyses of *N*-Glycoside Hydrolysis and *N*-Glycoside Transfer. *Chem. Rev. (Washington, DC, U. S.)* **2006**, *106*, 506−555.
(69) Bjørås, M.; Luna, L.; Johnson, B.; Hoff, E.; Haug, T.; Rognes, T.; Seeberg, E. Opposite Base-dependent Reactions of a Human Base Excision Repair Enzyme on DNA Containing 7,8-Dihydro-8-oxoguanine and Abasic Sites. *EMBO J.* **1997**, *16*, 6314−6322.
(70) Dong, J.; Drohat, A. C.; Stivers, J. T.; Pankiewicz, K. W.; Carey, P. R. Raman Spectroscopy of Uracil DNA Glycosylase-DNA Complexes: Insights into DNA Damage Recognition and Catalysis. *Biochemistry* **2000**, *39*, 13241−13250.
(71) Brinkmeyer, M. K.; Pope, M. A.; David, S. S. Catalytic Contributions of Key Residues in the Adenine Glycosylase MutY Revealed by pH-Dependent Kinetics and Cellular Repair Assays. *Chem. Biol.* **2012**, *19*, 276−286.
(72) Norman, D. P. G.; Bruner, S. D.; Verdine, G. L. Coupling of Substrate Recognition and Catalysis by a Human Base-Excision DNA Repair Protein. *J. Am. Chem. Soc.* **2001**, *123*, 359−360.
(73) Bjørås, M.; Seeberg, E.; Luna, L.; Pearl, L. H.; Barrett, T. E. Reciprocal "Flipping" Underlies Substrate Recognition and Catalytic Activation by the Human 8-Oxo-guanine DNA Glycosylase. *J. Mol. Biol.* **2002**, *317*, 171−177.
(74) Banerjee, A.; Yang, W.; Karplus, M.; Verdine, G. L. Structure of a Repair Enzyme Interrogating Undamaged DNA Elucidates Recognition of Damaged DNA. *Nature (London, U. K.)* **2005**, *434*, 612−618.
(75) Radom, C. T.; Banerjee, A.; Verdine, G. L. Structural Characterization of Human 8-Oxoguanine DNA Glycosylase Variants Bearing Active Site Mutations. *J. Biol. Chem.* **2007**, *282*, 9182−9194.
(76) Hunter, K. C.; Wetmore, S. D. Environmental Effects on the Enhancement in Natural and Damaged DNA Nucleobase Acidity Because of Discrete Hydrogen-Bonding Interactions. *J. Phys. Chem. A* **2007**, *111*, 1933−1942.
(77) McConnell, T. L.; Wheaton, C. A.; Hunter, K. C.; Wetmore, S. D. Effects of Hydrogen Bonding on the Acidity of Adenine, Guanine, and Their 8-Oxo Derivatives. *J. Phys. Chem. A* **2005**, *109*, 6351−6362.
(78) Millen, A. L.; Archibald, L. A. B.; Hunter, K. C.; Wetmore, S. D. A Kinetic and Thermodynamic Study of the Glycosidic Bond Cleavage in Deoxyuridine. *J. Phys. Chem. B* **2007**, *111*, 3800−3812.
(79) Le Bihan, Y. V.; Angeles Izquierdo, M.; Coste, F.; Aller, P.; Culard, F.; Gehrke, T. H.; Essalhi, K.; Carell, T.; Castaing, B. 5-Hydroxy-5-methylhydantoin DNA Lesion, a Molecular Trap for DNA Glycosylases. *Nucleic Acids Res.* **2011**, *39*, 6277−6290.